NJC

New Journal of Chemistry

A journal for new directions in chemistry

Accepted Manuscript

This article can be cited before page numbers have been issued, to do this please use: J. Custodio, A. Moura, M. O. de Moraes, C. Perez and H. Napolitano, *New J. Chem.*, 2020, DOI: 10.1039/C9NJ05612B.

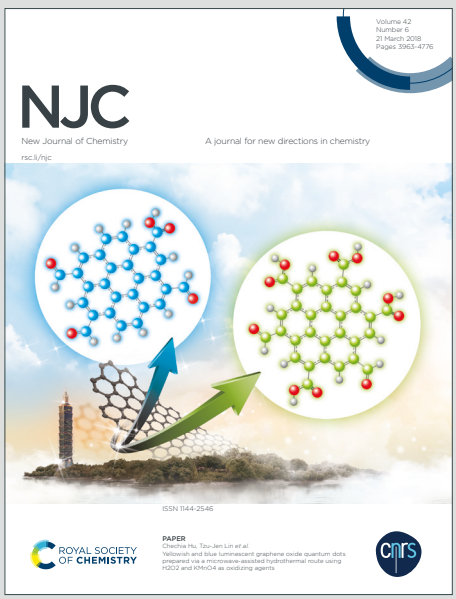

On the *In Silico* and *In Vitro* Anticancer Activity of Sulfonamide Chalcones: Potential JNKK3 Inhibitors

Jean M. F. Custodio[a,b]*, Andrea F. Moura[c,d], Manoel O. de Moraes[c], Caridad N. Perez[b] and Hamilton B. Napolitano[e]

[a]Department of Chemistry and Biochemistry, University of Notre Dame, Notre Dame, IN, 46556, United States

[b]Instituto de Química, Universidade Federal de Goias, Goiania, Goias, 74690-900, Brazil

[c]Núcleo de Pesquisas e Desenvolvimento de Medicamentos, Universidade Federal do Ceará, Fortaleza, Ceará, 60430-275, Brazil

[d]Núcleo de Pesquisa em Biotecnologia e Biodiversidade - BIOTEC, Universidade Federal do Piauí, Parnaíba, Piauí, 64200500, Brazil

[e]Ciências Exatas e Tecnológicas, Universidade Estadual de Goiás, Anapolis, Goias, 75132-903, Brazil

Correspondence email: jeanmfcustodio@gmail.com

Abstract Science is constantly looking for new strategies to combat tumor progression and improve patient care due to increasing cancer incidence and high mortality. Although many chalcones analogues have been synthesized and studied because of their activity against tumor cell growth, the use of hybrid compounds containing both sulfonamides and chalcone moieties for this purpose is still scarce. Hereby, this work proposes a series of sulfonamide chalcones presenting biological potential against this disease. After experimentally tested, these compounds showed cytotoxicity against tumor cell lines, SF-295 and PC-3, which motivated us to investigate the possible structural bases for this action. Topological analyses were carried out through Hirshfeld analysis to assign intermolecular interactions sites important for protein-ligand analysis. To identify potential targets, the synthesized compounds were submitted to a structure-based pharmacophoric screening, which suggest strong potential activity as Mitogen-activated protein kinase 10 (JKN3) inhibitors. Considering these results, these compounds were docked within the JKN3 active site. Our hypothesis that these compounds achieve their biological potential by inhibiting JKN3 protein is reinforced when their energies of ligand-protein interaction were compared to co-crystallized ligands: they showed similar or even lower binding energies. Finally, the energy of the different conformations (solid phase, aqueous phase and within the protein active site) of these sulfonamide chalcones was investigated from

theoretical calculations. Our findings enable further studies on more sulfonamide chalcone analogues toward the development of new anticancer drugs.

1. Introduction

Science is constantly looking for new strategies to combat tumor progression and improve patient care due to increasing cancer incidence and high mortality. However, the results are not always satisfactory, with high rates of tumor recurrence and metastasis, as well as induction of many side effects. Therefore, research based on targeted target therapy has grown significantly. Studying the different characteristics of cancer cells has resulted in the development of targeted target drugs[1], especially those involving protein kinases, enzymes encoded by the human genome.

Among these protein kinases, the mitogen-activated protein kinases (MAP kinases) are a family of kinases that respond to oncogenic mutational events and regulate proliferation and apoptosis as well as the metabolic reprogramming of tumor cells. In mammalians, three subfamilies of MAPKs are well-characterized: ERKs (extracellular signal-regulated kinases), p38 kinases and JNKs (c-Jun N-terminal kinase))[2]. The oncogenesis related with JNKs involves cell proliferation, survival, transformation, inflammation, migration and suppression of cell death disorders. Thereby, pharmaceutical industry has been developed new compounds that act as selective inhibitors of the JNKs[3]. The development of new molecules based on knowledge of the pathophysiology of diseases, the study of biochemical pathways and the selection of molecular targets in order to identify novel compounds with optimized and targeted biological activity, low toxicity and favorable therapeutic index has been encouraged[4,5].

Although many compound classes have been studied as JNK inhibitors, we are interested in using chalcones for this purpose due their chemistry, which provides many biological applicability for them[6–10]. Having a double bond in conjugation with carbonyl group, these α-β-unsaturated ketones are known by their potential as anti-cancer[11], anti-malarial[12], antimicrobial[13], anti-protozoal[14] and anti-HIV[15] agents. In order to search for new molecules more effective, new chalcones have been developed from the addition of organic groups, as substituents of aromatic rings, with known biological properties. Several substituents at different positions in the chemical structure of these molecules may determine different biological activities as well as specific mechanisms of action[16] .Sulfonamide

addition has been described, in which compounds, called sulfonamide chalcones, demonstrate several biological activities already reported, like antifilaria[17], antimalarial[18,19] and anticancer[20] , as well as α-glucosidase inhibitor[21], beta-secretase and acetylcholinesterase[22], carbonic anhydrase[23,24] and ecto-5'-nucleotidase and intestinal alkaline phosphatase[25].

Herein, we describe some previously synthesized sulfonamide chalcones (**I-IX**), discussing some structural aspects obtained from single crystal X-ray Diffraction (SCXRD). Their topological analysis was presented from Hirshfeld surfaces (HS), which shows potential intermolecular interaction sites important to protein ligand analysis. The biological potential against tumor cell lines, like glioblastoma (SF-295) and prostate adenocarcinoma (PC-3) was confirmed by cytotoxic assay. To identify their possible potential targets, these compounds were submitted to a structure-based pharmacophoric screening. Once identified the target, they were docked into the active site of the result target and their binding modes and energies were compared to the standard cocrystalized ligand. Finally, we investigated the energy of the different conformations (solid phase, aqueous phase and within the protein active site) from theoretical calculations.

2. Methodology

2.1. Crystallographic Model

The compound 2′N-(phenylsulfonyl)acetophenone (**a**) was synthesized from reaction between benzenesulfonyl chloride and 2-aminoacetophenone in dichloromethane medium (Scheme 1a). Then, sulfonamide chalcones **I-IX** were obtained from Claisen-Schmidt condensation between **a** and their respective benzaldehydes, following Scheme 1b. They were crystallized from saturated dichloromethane solutions. Suitable crystals of **I-IX** were mounted and collected using a Bruker *APEX*-II CCD diffractometer equipped with MoKα radiation, and were found to be crystallized under centrosymmetric space groups triclinic $P\bar{1}$ (**IV** and **V**); monoclinic $P2_1/c$ (**I**, **VI**, **IX** and **VIII**); $P2_1/n$ (**VII** and **III**); and $C2/c$ (**II**). Compounds **I-IV** and **VI-IX** have one molecule per asymmetric unit (AU), while **V** presents two molecules per AU. All hydrogen atoms were refined following the ridding model, with fixed U_{iso} at 1.2 times U_{eq}(C) (for aromatic and CH_2 groups) and 1.5 times U_{eq}(C) (for methyl groups). Crystallographic data for compounds **I-IX** were deposited at Cambridge

View Article Online
DOI: 10.1039/C9NJ05612B

Crystallographic Data Centre (CCDC) under codes 1868826, 1868827, 1850083, 1949070, 1949072, 1868828, 1904244, 1904245 and 1949073, respectively.

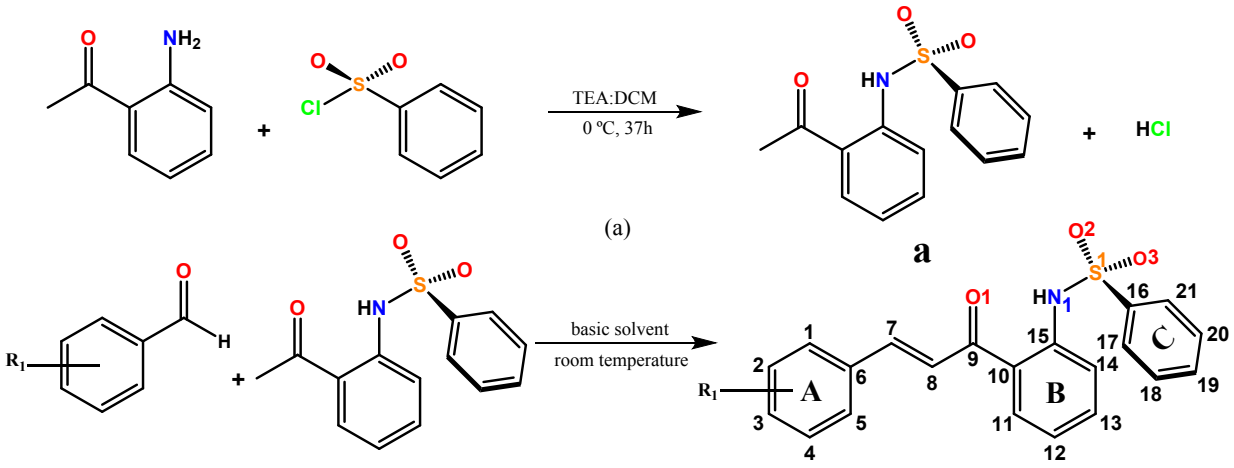

R_1 = I: *o*-Cl; II: *o*-F; III: *o*-Br; IV: *p*-Cl; V: *p*-Br; VI: *p*-F; VII: *o*-Methoxy; VIII: *m*-Nitro; IX: *p*-Ethoxy

(b)

Scheme 1 Synthesis of intermediate **a** (a) and sulfonamide chalcones **I-IX** (b) with numbering scheme used for them.

The intermolecular interactions observed stabilizing the crystal packing of **I-IX** were analyzed from their HS through Crystal Explorer[26] program. Weak C–H···O interactions were qualitatively analyzed from d_{norm} HS, which is based on the combination of d_e (distance from an outer nucleus to the HS) and d_i (distance from an inner nucleus to the HS) in a color-based scale ranging from blue (longest distances) to red (shortest distances)[27]. Also, hydrophobic interactions such as C–H···π and π···π were studied from shape index HS, which shows both their acceptor and donor regions as red concave and blue convex shapes, respectively[28–30]. Finally, these interactions were quantitatively analyzed from the fingerprint plots, showing a 2D representation of *de* and *di* of each contact type[31].

2.2. Antitumor tests

The human tumor cells lines used in this work were SF-295 (glioblastom) and PC-3 (prostate adenocarcinoma), which were kindly provided by the National Cancer Institute (Bethesda, MD, USA). These cells were cultured in RPMI1640 medium and supplemented with 10% fetal bovine serum (2 mM glutamine, 100 U.mL^{-1} penicillin), and 100 µg.mL^{-1} streptomycin at 37 °C with 5% CO_2. All cell lines were cultured in humidified atmosphere of 5% CO_2 at 37 °C. Stock solution of **I-IX** and doxorubicin (positive control) were solubilized in DMSO for cytotoxic assay. Their cytotoxicity against above mentioned cell lines was tested using MTT assay. Cells were plated in 96-well plates and treated with 25 µg.mL^{-1} of

compounds **I-IX** to initial screening. At the end of 72 h of incubation, the plates were centrifuged, and the supernatant was removed and replaced with fresh medium (150 µL) containing MTT (0.5 mg/mL). Cells were incubated for 3 hours. Tumor cell growth was quantified by the ability of living cells to reduce the yellow dye 3-(4,5-dimethyl-2-thiazolyl)-2,5-diphenyl-2H-tetrazolium bromide (MTT) to a purple formazan product by metabolically active cells (MOSMANN, 1983). The MTT formazan product was dissolved in 150 µL of DMSO, and the absorbance was measured using a multiplate reader (Spectra Count, Packard, Ontario, Canada) at 595 nm.

Cell growth inhibition percentage (GI%) was calculated. In sequence, they were retested using MTT assay for determination of half-maximal inhibitory concentration (IC50 value). For this, increasing concentrations of **I-IX** (0.19 - 25 $\mu g.mL^{-1}$) were used for test. DMSO was used as negative control and doxorubicin (0.04 - 5 $\mu g.mL^{-1}$) was used as a positive control. The GI% was determined based on the negative control. The IC50 values and their 95% confidence intervals (CI 95%) were obtained by non-linear regression using GraphPad Prism 5.0 (Intuitive Software for Science, San Diego, CA).

2.3. Structure-based pharmacophoric screening

The structure-based potential drug target identification was obtained from a reversed pharmacophore matching approach using the online tool PharMapper[32]. PharMapper results are reliable because they are derived from more than 23 000 proteins covering 16 159 *druggable* pharmacophore models and 51 431 ligandable pharmacophore models[32] present in the databases TargetBank, DrugBank, BindingDB and PDTD. As input, the maximum generated conformations for each compound was set to 300 and only human protein targets were considerate.

2.4. Molecular Docking

Aiming an improved understanding on how compounds **I-VIII** interact with the found target (Mitogen-activated protein kinase 10, JNK3), we propose a molecular modeling of these synthetic molecules. The MarvinSketch v.6.3.1 program (ChemAxon, Budapest, Hungary, http://www.chemaxon.com) was used to build the 3D structure of **I-VIII** at neutral condition (pH = 7.4). In addition, OMEGA v.3.0.0.1 software[33,34] was used to generate up to 69 conformers, which AM1-BCC charges[35] were calculated through QUACPAC v.1.7.0.2[36]. The 3D structure of JNK3 enzyme was obtained from the Protein Data Bank (PDB) and was

also prepared at pH = 7.4 and its protonation states were predicted by H++ server[37,38]. Molecular docking procedures were carried out on AutoDock-Vina software[39].

2.5. Theoretical Calculations

Chemical conformations of **I-IX** were calculated in the solid state (SS), aqueous-simulated medium (AS) and that observed from docking results (DS). The atomic coordinates were taken from their respective crystallographic model. For SS, all hydrogen atoms were optimized, for DS all atoms were totally optimized using dielectric constant ε=78.3553 (water) and for DS, the single point energy was calculated from docking results output. All calculations were performed using the density functional theory (DFT) at exchange-correlation functional M062X and basis set 6-311++G(d,p).

3. Results and Discussion

3.1. Solid State Comments

Figure 1 presents the overlay of compounds **I-IX**, obtained by overlapping aromatic ring B. These compounds have different conformations, and overall differences are regarding both the planarity (dihedral angles and angle and formed between the rings A and B) and conformation of ring C. Compounds **I** and **III** differ each other by an isomorphic substitution of the chlorine by a bromine at ring A. Also, there is no noticeable difference on molecular structures of **IV** and **IX**. The conformation of the sulfonyl ring is derived from a rotation of the C15–N1 σ-bond, so that the dihedral angle C14–C15–N1–S1 was analyzed for **I-IX** ($\omega_{\boldsymbol{I}}$= -5.93; $\omega_{\boldsymbol{II}}$= 28.26; $\omega_{\boldsymbol{III}}$= -6.12; $\omega_{\boldsymbol{IV}}$= -41.43; $\omega_{\boldsymbol{V}}$= -34.49; $\omega_{\boldsymbol{VI}}$= -23.73; $\omega_{\boldsymbol{VII}}$= -49.76; $\omega_{\boldsymbol{VIII}}$= 4.97; $\omega_{\boldsymbol{IX}}$= -41.94). These values evidence the conformational variability of the ring C, which range from syn-periplanar (**I-III**, **VI** and **VII**) to syn-clinal (**IV-V**, **VII** and **IX**).

View Article Online
DOI: 10.1039/C9NJ05612B

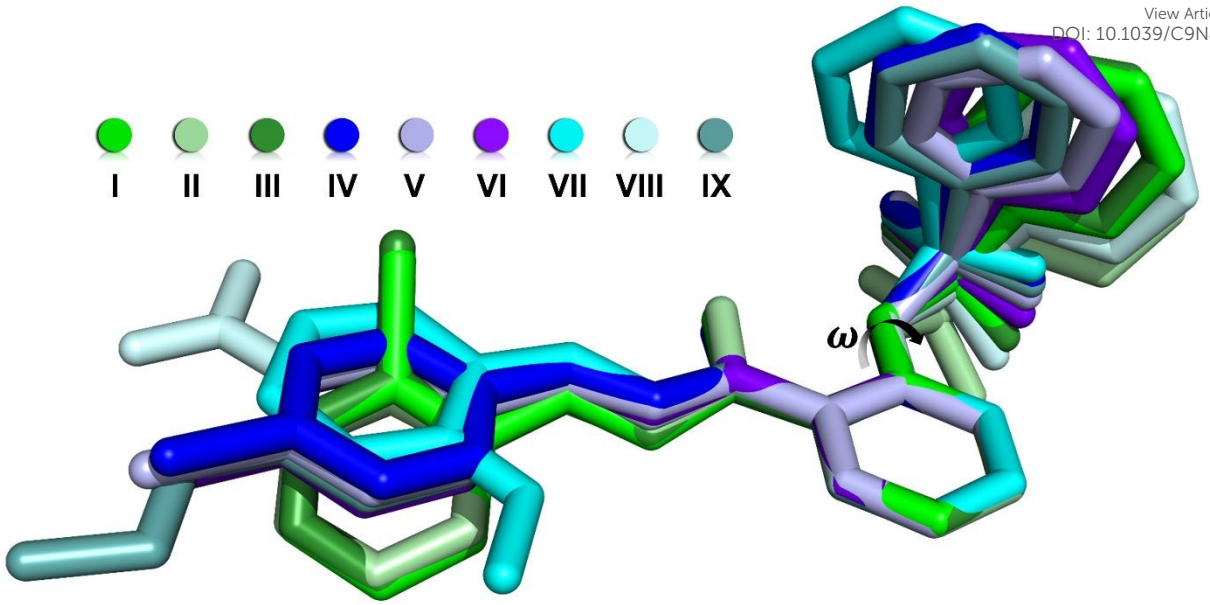

Figure 1 Overlay of compounds I-IX in solid phase, showing the main difference of their conformations.

Further information about intermolecular interactions observed for **I-III** are inferred from their d_{norm} HS and respective 2D fingerprint plots in Figure 2a, Figure 2b and Figure 2c. Figure 2a shows the C–H···O interactions that stabilizes the crystal packing of **I**, highlighting them as red spots on both HS points of view where "a" and "d" mean their acceptor and donor regions, respectively. The strongest interaction, C21–H21···O1, assembles **I** in dimers involving the carbonyl group. For **II**, the strongest interaction involves the atoms O2, O3, H8 and H5 in a chain with similar d_e and d_i of **I**. Although with similar distances for their strongest interaction (Figure 2b), the weaker interactions of **I** (C5–H5···O3 and C13–H13···O2) are stronger than those observed for **II** (C18–H18···F1 and C3–H3···O2) and play an important role in its crystal packing. Figure 2c confirms that the crystal packing of **III** is also stabilized by a dimer through interaction C17–H17···O1, an interaction with medium distance (C5–H5···O2) and one weak interaction (C13–H13···O3). The ranges used for the d_{norm} HS calculation and distances observed for each compound is presented in Table 1.

View Article Online
DOI: 10.1039/C9NJ05612B

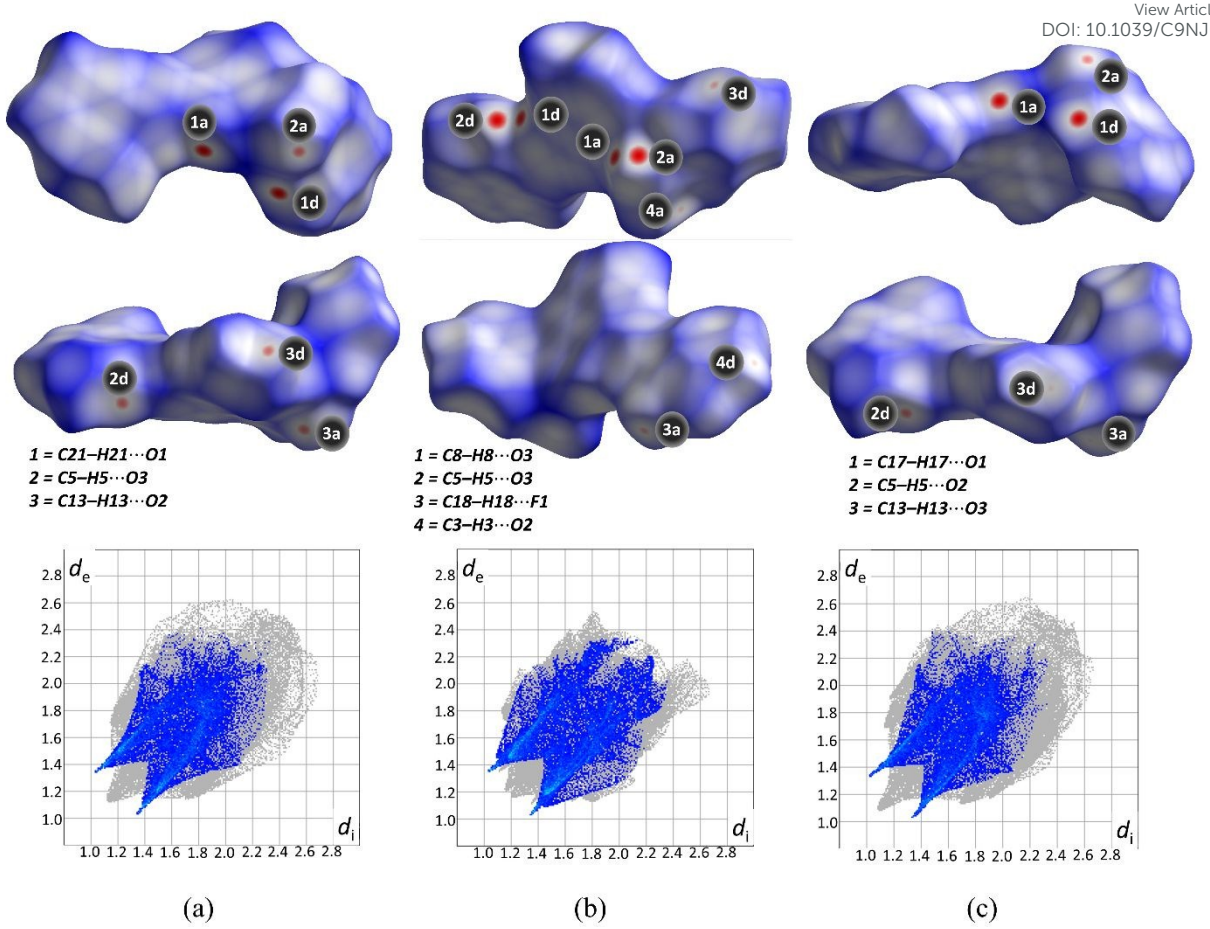

Figure 2 d_{norm} HS and 2D fingerprint plots showing the C–H···O interactions of (a) I, (b) II and (c) III. Acceptor and donor regions are represented by "a" and "d", respectively.

Table 1 Ranges used for the d_{norm} HS calculation and distances observed for compounds **I-IX**.

Compound	Range used for d_{norm} HS (Å)	Selected Contacts	Approximated Donor Distances (Å)		Approximated Acceptor Distances (Å)	
			d_i	d_e	d_i	d_e
I	-0.1504 – 1.3826	C21–H21···O1	1.0	1.3	1.3	1.0
II	-0.1500 – 1.5279	C8–H8···O3	1.0	1.3	1.3	1.0
		C5–H5···O3	1.0	1.3	1.3	1.0
III	-0.1595 – 1.5010	C17–H17···O1	0.9	1.2	1.2	0.9
		C5–H5···O2	1.2	1.4	1.4	1.2
		C13–H13···O3	1.3	1.5	1.5	1.3
IV	-0.1823 – 1.4464	C4–H4···O1	1.0	1.3	1.3	1.0
		C8–H8···O2	1.0	1.4	1.4	1.0
		C13–H13···O3	1.2	1.5	1.5	1.2
V **Vα**	-0.2511 – 1.2786	C5–H5···O2	0.9	1.3	1.3	0.9
		C8–H8···O2	1.1	1.4	1.4	1.1
		C4–H4···O1	1.2	1.5	1.5	1.2
		C2*–H2*···C6	1.1	1.8	1.8	1.1
		C17*–H17*···C13	1.1	1.6	1.6	1.1
Vβ	-0.1778 – 1.3551	C8*–H8*···O2*	1.0	1.3	1.3	1.0

		C19*–H19*···C6*	1.2	1.7	1.7	1.2
		C19*–H19*···C1*	1.1	1.7	1.7	1.1
		C4*–H4*···O1*	1.2	1.5	1.5	1.2
VI	-0.1731 – 1.3684	C12–H12···C20	1.1	1.6	1.6	1.1
		C20–H20···O1	1.4	1.6	1.6	1.4
		C5–H5···O2	1.1	1.5	1.5	1.1
VII	-0.1445 – 1.2976	C22–H22B···O2	1.2	1.5	1.5	1.2
		C21–H21···O1	1.1	1.3	1.3	1.1
		C22–H22B···O2	1.1	1.4	1.4	1.1
		C9···C9	1.6	1.6	1.6	1.6
VIII	-0.2927 – 1.4930	C5–H5···O2	1.0	1.1	1.1	1.0
		C8–H8···O2	1.0	1.1	1.1	1.0
		C11–H11···O2	1.0	1.1	1.1	1.0
		C19–H19···O4	1.4	1.6	1.6	1.4
		C7–H7···O3	1.2	1.4	1.4	1.2
		C20–H20···O3	0.9	1.1	1.1	0.9
IX	-0.2045 – 1.4787	C5–H5···O2	1.0	1.1	1.1	1.0
		C8–H8···O2	0.9	1.0	1.0	0.9
		C11–H11···O2	1.0	1.1	1.1	1.0

The crystal packing of compounds **I-III** are also stabilized by both C–H···π and π···π interactions, which play an important role in several fields, such as the packing of aromatic molecules in crystals and complexation in many host-guest systems[40]. On the shape index HS, these interactions are represented as one red concave region and one blue convex region over the aromatic ring and H atom, respectively (C–H···π interactions) and as two red and blue triangular shapes over aromatic rings (π···π interactions). On the other hand, C–H···π interactions are represented by C–H contacts in the 2D fingerprint plot, while π···π interactions are represented by C–C contacts. Two molecules of I are related by the interaction Cg_1···Cg_2 (Figure 3a). Also, there are two molecules of I related by the interaction C3–H3···Cg_3. For **II**, the π···π interactions involve Cg_1···Cg_1 and Cg_2···Cg_2, while the C–H···π interaction occurs between C11 and Cg_3 as shown in Figure 3b. Figure 3c shows that, similarly to **I**, the crystal packing of **III** is also stabilized by one Cg_1···Cg_2 and one C3–H3···Cg_3 interactions. Details on distances involved in C–H···π and π···π interactions observed for compounds **I-IX** are given on Table 2.

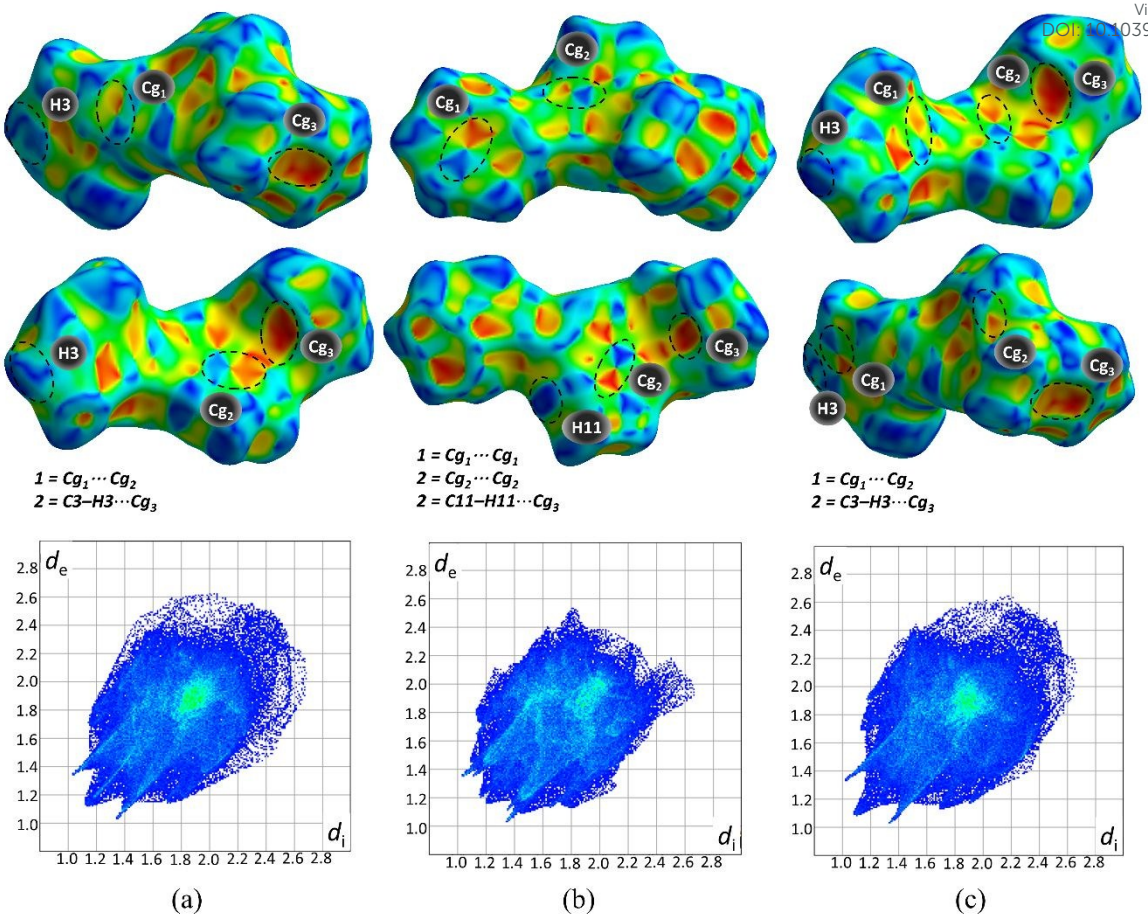

Figure 3 Representation of C–H···π and π···π interactions stabilizing the crystal packings of (a) **I**, (b) **II** and (c) **III**. Both shape index HS and 2D fingerprints plots are shown. Blue and red represent donor and acceptor regions, while other colors represent intermediate states.

Table 2 Distance of C–H···π and π···π interactions observed for compounds I-IX. Cg_1, Cg_2 and Cg_3 are the center of gravity of aromatic rings A, B and C, respectively.

Compound	Selected Contacts	π···π		C–H··· π		
		$d_{Cg\cdots Cg}$ (Å)	Slippage (Å)	$d_{H\cdots Cg}$(Å)	$d_{C\cdots Cg}$ (Å)	$\angle_{C3\text{-}H3\cdots Cg}$ (°)
I	$Cg_1\cdots Cg_2$	3.9076	1.238	–	–	–
	C3–H3···Cg_3	–	–	3.25	4.086	150
II	$Cg_1\cdots Cg_1$	3.9034	1.281	–	–	–
	$Cg_2\cdots Cg_2$	4.0181	1.515	–	–	–
	C11–H11···Cg_3	–	–	2.94	3.612	130
III	$Cg_1\cdots Cg_2$	3.8863	1.269	–	–	–
	C3–H3···Cg_3	–	–	2.94	3.612	130
IV	$Cg_1\cdots Cg_1$	3.7773	1.200	–	–	–

View Article Online
DOI: 10.1039/C9NJ05612B

		$Cg_2 \cdots Cg_2$	3.9342	1.581	–	–	
		C3–H3$\cdots Cg_3$	–	–	2.81	3.740	174
V	**Vα**	C2*–H2*$\cdots Cg_1$	–	–	2.79	3.604	154
		C17*–H17*$\cdots Cg_2$	–	–	2.76	3.591	149
		Cg_1*$\cdots Cg_1$*	3.8339	1.495	–	–	–
	Vβ	C19*–H19*$\cdots Cg_1$*	–	–	2.70	3.559	155
		C21–H21$\cdots Cg_2$*	–	–	2.86	3.721	155
VI		$Cg_1 \cdots Cg_1$	4.4063	2.311	–	–	–
		$Cg_2 \cdots Cg_2$	4.0974	1.861	–	–	–
VII		$Cg_1 \cdots Cg_2$	3.8971	1.513	–	–	–
VIII		$Cg_1 \cdots Cg_2$	3.8178	1.329	–	–	–
		C3–H3$\cdots Cg_3$	–	–	2.96	3.794	144
IX		$Cg_1 \cdots Cg_2$	3.8882	1.370	–	–	–
		C22–H22$\cdots Cg_1$	–	–	2.903	3.763	148
		C21–H21$\cdots Cg_2$	–	–	2.839	3.707	156

For **IV**, there are two strongest interactions observed the d_{norm} HS: C4–H4···O1 and C8–H8···O2 (Figure 4a). Its crystal packing is also stabilized by a different dimer regarding compounds **I-III**. This dimer involves atoms C13 and O3 and, based on its intermolecular distances, plays a secondary role on the crystal packing. Compound **V** has two conformers per asymmetric unit, here named **V**α and **V**β. Thus one d_{norm} HS was generated one d_{norm} HS for each conformer, shown in Figure 4b (**V**α) and Figure 4c (**V**β). For **V**α, there are two strongest interactions involving C5–H5···O2 and C8–H8···O2. Also, weaker interactions stabilize the crystal packing of **V** relating two **V**α conformers (C4–H4···O1) and one **V**α with one **V**β conformers (C2*–H2*···C6 and C17*–H17*···C13) conformers. There are one stronger interaction (C8*–H8*···O2*) and three weaker interactions (C19*–H19*···C6*, C19*–H19*···C1* and C4*–H4*···O1*) relating two **V**β molecules. The d_{norm} HS calculated for **VI** (Figure 4d) shows that the strongest directional interaction involves two C atoms (C12–H12···C20), different from compounds **I-V**. There are also two C–H···O interactions observed for **VI**, C20–H20···O1 and C5–H5···O2.

View Article Online
DOI: 10.1039/C9NJ05612B

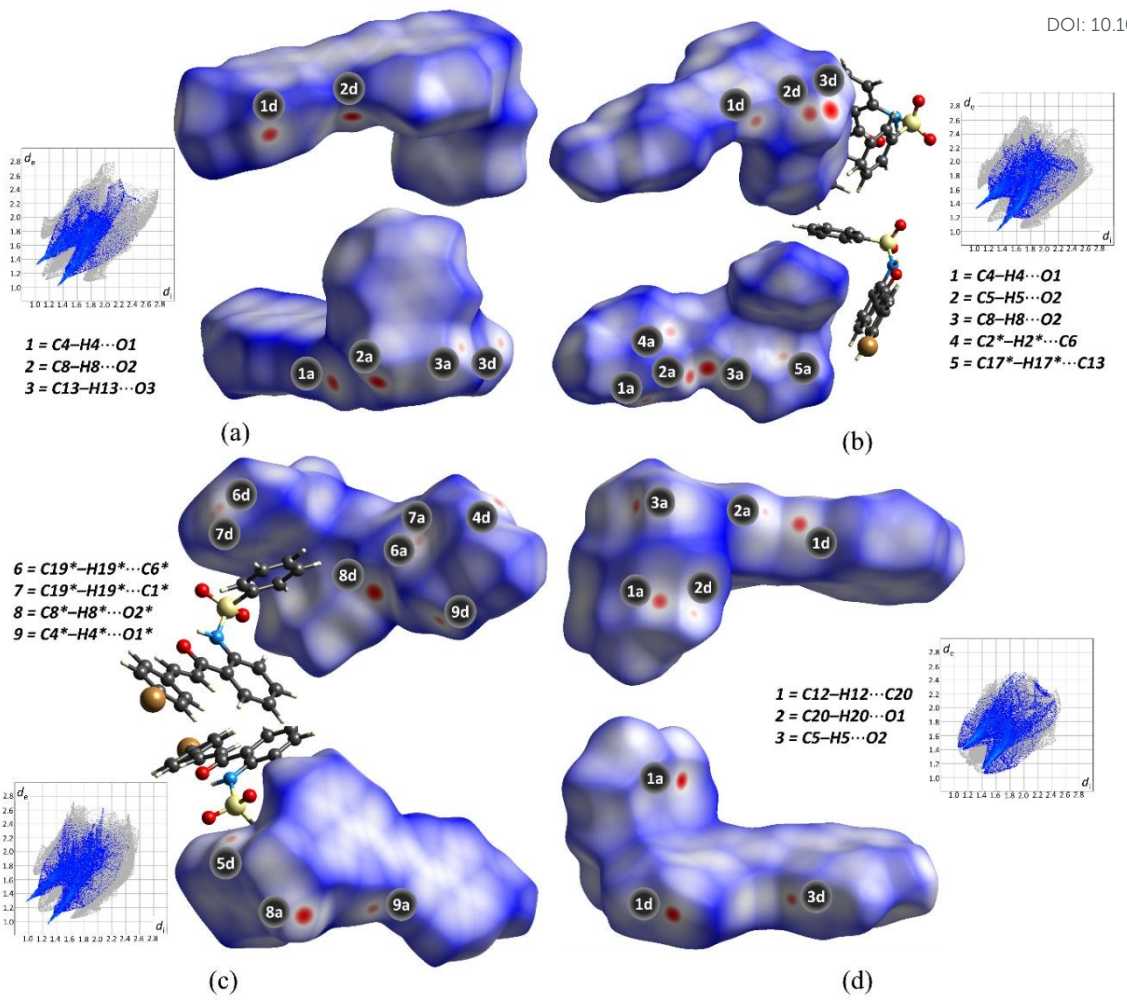

Figure 4 d_{norm} HS and 2D fingerprint plots showing C–H···O and C–H···C interactions of (a) **IV**, (b) **Vα**, (c) **Vβ** and (d) **VI**. Acceptor and donor regions are represented by "a" and "d", respectively.

The shape index HS calculated for **IV** shows that these molecules are assembled through both C–H···π and π···π interactions (Figure 5a). Molecules of **IV** are stacked by means of the Cg_1···Cg_1 interaction, while molecules of **IV** are stacked throughout Cg_2···Cg_2 interaction. There is also one interaction involving C3–H3···Cg_3, which forms a centrosymmetric dimer. There are only C–H···π interactions involving **V**α (Figure 5b). Centroids Cg_1 and Cg_2 act as acceptors for the intermolecular interactions C2*–H2*···Cg_1 and C17*–H17*···Cg_2. On the other hand, Cg_1* and Cg_2* are involved both in π···π and C–H···π interactions (Figure 5c) for **V**β. For compound **VI**, only π···π interactions were observed involving both Cg_1 and Cg_2 (Figure 5d).

View Article Online
DOI: 10.1039/C9NJ05612B

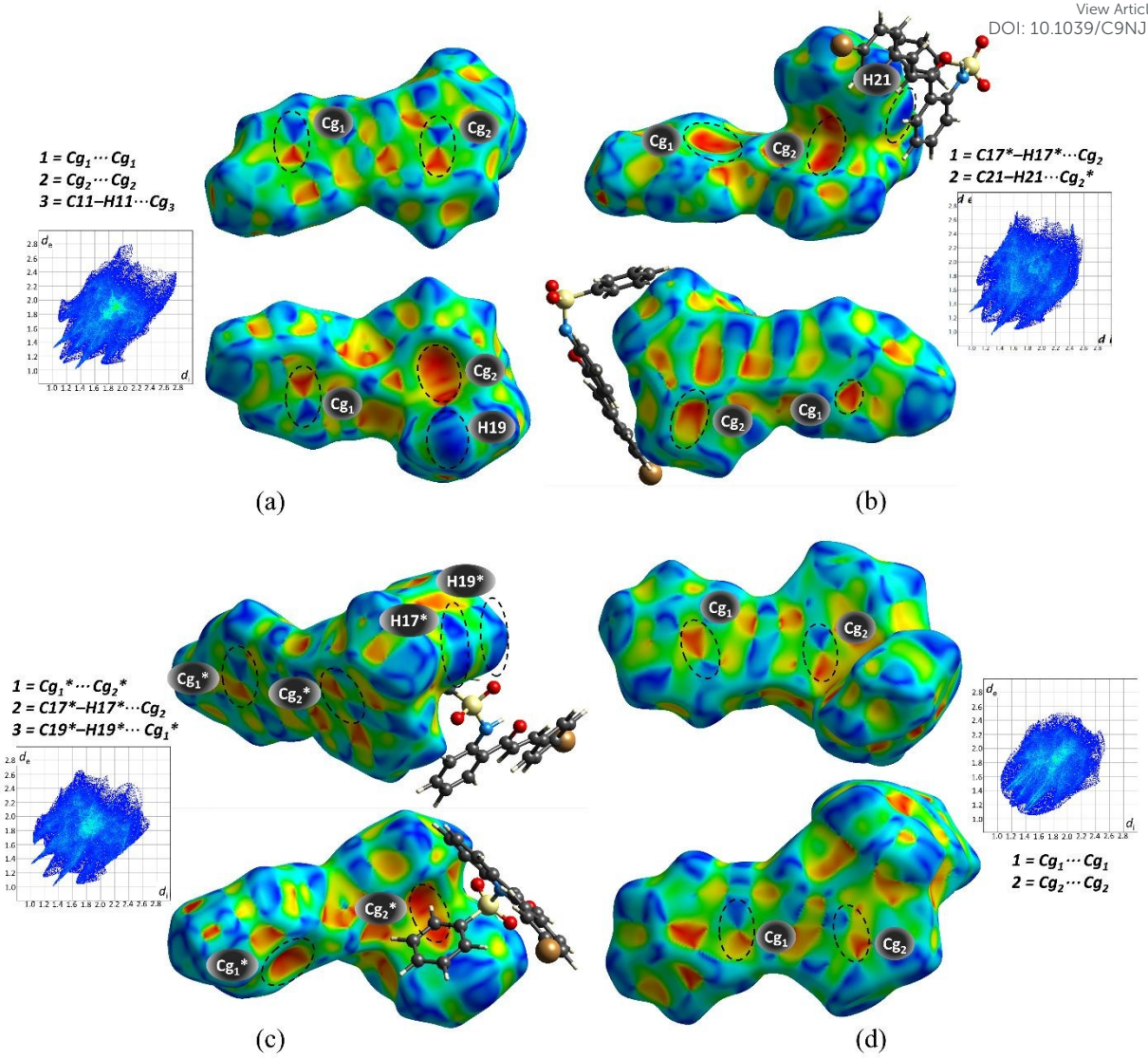

Figure 5 Representation of C–H···π and π···π interactions stabilizing the crystal packing of (a) **IV**, (b) **Vα**, (c) **Vβ** and (d) **VI**. Both shape index HS and 2D fingerprints plots are shown.

The d_{norm} HS calculated for **VII** evidences that there are three C–H···O (C22–H22B··· O2; C21–H21···O1 and C22–H22B···O2) interactions and one unusual C9···C9 contact stabilizing the crystal packing (Figure 6a). For both **VIII** (Figure 6b) and **IX** (Figure 6c), there is the same trifurcated interaction pattern involving C5–H5···O2, C8–H8···O2 and C11–H11···O2, in which that involving C5 is dominant. There are three more C–H···O interactions stabilizing the crystal packing of **VIII**: C19–H19···O4.

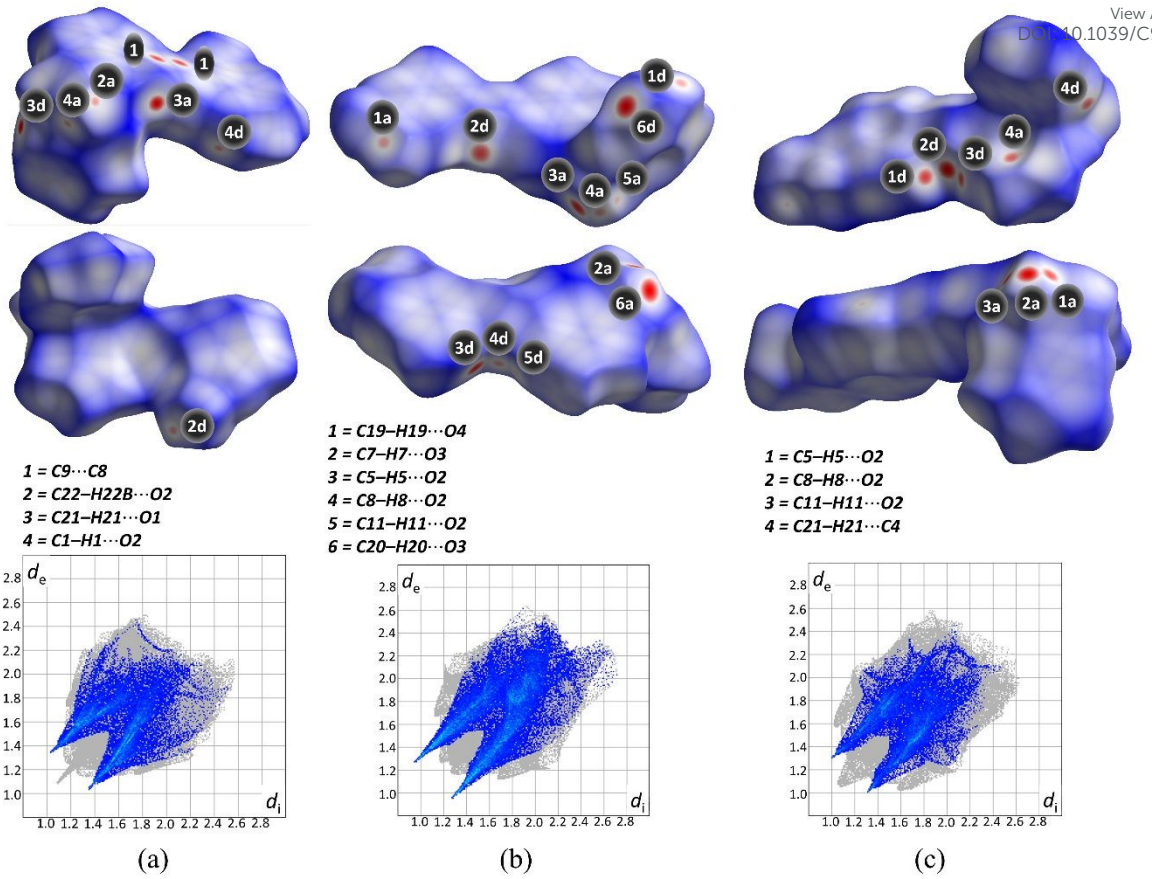

Figure 6 d_{norm} HS and 2D fingerprint plots showing the C–H···O interactions of (a) **VII**, (b) **VIII** and (c) **IX**. Acceptor and donor regions are represented by "a" and "d", respectively.

The shape index HS was calculated for **VII** (Figure 7a), **VIII** (Figure 7b) and **IX** (Figure 7c) to analyze how these molecules pack and what kind of contacts stabilize their crystal packing. The crystal packing of **VII** is stabilized by π-stacking interactions involving both Cg_1 and Cg_2. Figure 7b shows that the crystal packing of **VIII** is stabilized by one Cg_1 ···Cg_2 stacking and one C–H···π interaction involving C3–H3···Cg_3, similar to **IV**. Finally, the crystal packing of compound **IX** was found to be stabilized by a Cg_1···Cg_2 stacking. For this compound, both Cg_1 and Cg_2 act also as acceptors for interactions C22–H22···Cg_1 and C21–H21···Cg_2.

View Article Online
DOI: 10.1039/C9NJ05612B

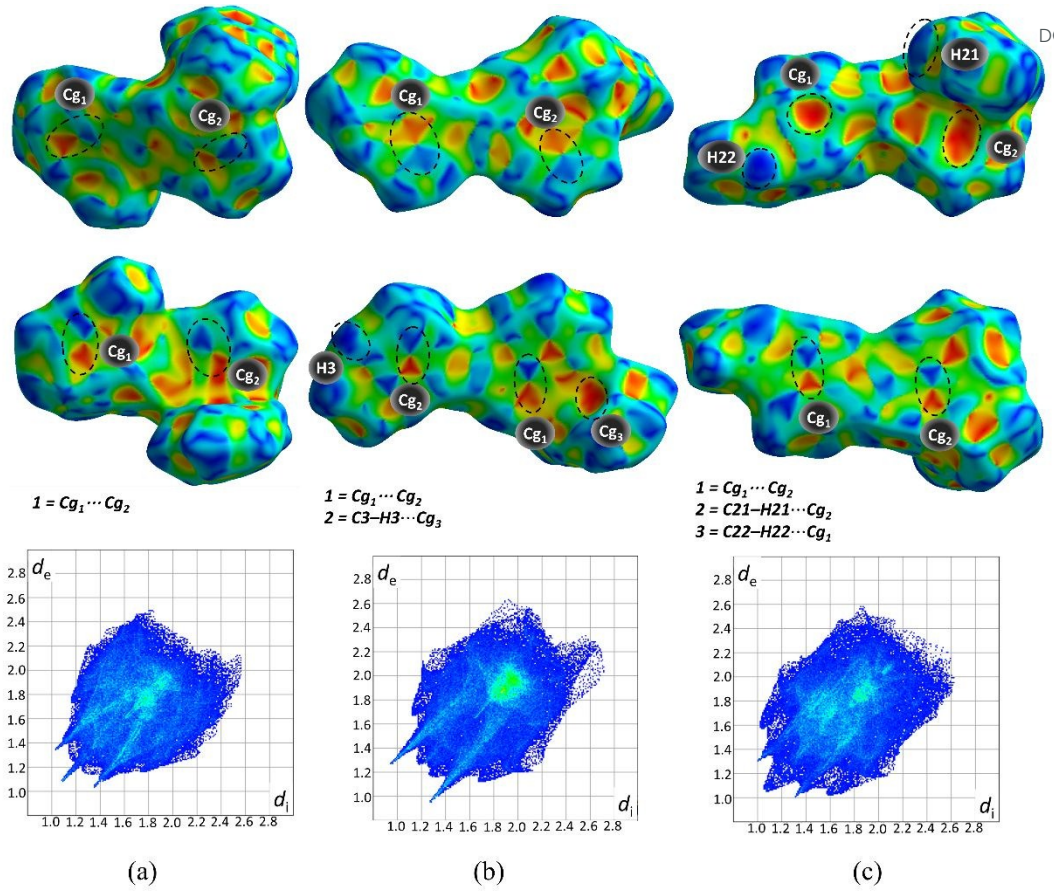

Figure 7 Representation of C–H···π and π···π interactions stabilizing the crystal packings of (a) **VII**, (b) **VIII** and (c) **IX**. Both shape index HS and 2D fingerprints plots are shown.

3.2. Cytotoxic Assay

The addition of chemical clusters to molecules with known biological activity through chemical synthesis has been frequent in order to determine different biological activities as well as specific mechanisms of action. In order to find new molecules more effective against a specific therapeutic target, new chalcones have been developed from the addition of organic groups, as substituents of aromatic rings, with known biological properties[16]. The cytotoxicity activity of sulfonamide chalcones previously synthesized by our group has been reported in other studies already published[41–43]. In this study, nine sulfonamide chalcones were tested against the human tumor cell lines SF-295 and PC-3 to verify *in vitro* cytotoxicity activity, using MTT assay. Among the sulfonamide chalcones tested, **I-VIII** were cytotoxic, with GI% greater than or equal to 75% against at least one tested tumor cell line. Only **IX** showed no cytotoxicity against tested tumor cell lines (Table 3).

Table 3 Cytotoxicity of Sulfonamide chalcones against two tumor cell lines. GI% values determined by MTT-assay using a concentration of 25 μg.mL^{-1} after 72 h of incubation. Doxorubicin was used as positive control using a concentration of 5 μg.mL^{-1}. Values are the average from three independent experiments shown with standard error.

Compound	SF-295	PC-3
I	82.6 ± 1.9	99.0 ± 0.7
II	83.2 ± 11.5	74.6 ± 22.4
III	79.8 ± 11.8	75.8 ± 22.9
IV	85.8 ± 10.8	77.5 ± 21.6
V	91.4 ± 0.6	99.4 ± 0.4
VI	73.8 ± 19.7	73.9 ± 24.7
VII	86.4 ± 10.5	77.7 ± 20.9
VIII	63.5 ± 1.1	77.9 ± 3.4
IX	39.6 ± 0.2	43.8 ± 3.7
Doxorubicin	79.3 ± 0.5	89.4 ± 0.2

Sulfonamide chalcones **I-VIII** were tested again using serial concentrations ranged 0.19 to 25 μg.mL^{-1} to determine IC_{50} values (Table 4). The tested compounds showed IC_{50} values ranging from 2.1 to 7.9 μg.mL^{-1} against two tested tumor cell lines. Among these active compounds, compound **IV** had the lowest IC_{50} values (2.1 and 2.4 μg.mL^{-1} against SF-295 and PC-3, respectively). In a previous study, carried out by our group, cytotoxicity of these molecules was evaluated against HCT-116, with IC50 values ranging from 2.4 to 7.5 μg.mL^{-1}.[44] With this, all these compounds are promising new drug candidate with anticancer activity.

Table 4 IC50 Values of compounds **I-VIII** against SF-295 and PC-3 tumor cell lines. IC50 Values and their 95% confidence intervals (CI 95%) were determined by MTT-assay using serial concentrations ranging to 0.19 to 25 μg.mL^{-1}, after 72 h of incubation. IC50 Values are from three independent experiments shown with 95% confidence intervals (CI 95%). Doxorubicin was used as positive control using serial concentrations ranging from 0.04 to 5 μg.mL^{-1}.

Compound	SF-295	PC-3
I	4.0 (3.1-5.1)	5.1 (4.8-5.4)
II	4.6 (4.0-5.3)	5.2 (4.8-5.6)
III	7.6 (6.5-8.9)	7.5 (6.8-8.3)
IV	2.1 (1.7-2.7)	2.4 (2.1-2.6)
V	5.0 (4.2-6.0)	5.9 (5.2-6.9)
VI	6.2 (4.3-8.9)	5.9 (5.2-6.7)
VII	7.1 (5.8-8.7)	6.9 (6.2-7.7)

View Article Online
DOI: 10.1039/C9NJ05612B

VIII	7.9 (6.5-9.7)	6.6 (5.7-7.5)
Doxorubicin	0.4 (0.3-0.5)	0.1 (0.1-0.2)

Recent studies have reported the chemical synthesis of new sulfonamide chalcones and their antitumor potential. The in vitro antitumor effect of these molecules has been described in some tumor cell lines, such as HEPG2 (liver cancer)[45], MCF-7 (breast cancer)[20], SF-295 (glioblastoma), PC-3 (prostate cancer) and HCT-116 (colorectal cancer)[46]. However, the mechanism of action of this class of molecules has not yet been explored. Based on these studies, molecules containing sulfonamide and chalcone moieties may lead to new hybrid architectures with improved biological profiles.

3.3. Molecular Docking

The wide range of biological activities of this compound class and the experimental results for compounds **I-VIII** motivated us study how our compounds acts to give the observed antitumor activity. First, we performed a structure-based potential drug target identification from a reversed pharmacophore matching approach using the online tool PharMapper[32]. PharMapper results are reliable because they are derived from more than 23,000 proteins covering 16,159 druggable pharmacophore models and 51,431 ligatable pharmacophore models[32] present in the databases TargetBank, DrugBank, BindingDB and PDTD. Also, seeking an improved accuracy, PharMapper also calculates a Fit Score for the pharmacophore model's ligands extracted from PDB and compares these Fit Scores to those obtained from analysed molecules[47,48].

Compounds **I-VIII** were submitted to PharMapper and the top-7 (those with better Fit Score) human proteins for each compound are presented in Table S1. The Mitogen-activated protein kinase 10 (JNK3, PDB code: 1PMV) was found to be a potential target for all analysed compounds, so that this protein was chosen for the binding mode analysis. Figure 8a shows this protein crystallized with dihydroanthrapyrazole (ATRP), a small molecule inhibitor [49].

View Article Online
DOI: 10.1039/C9NJ05612B

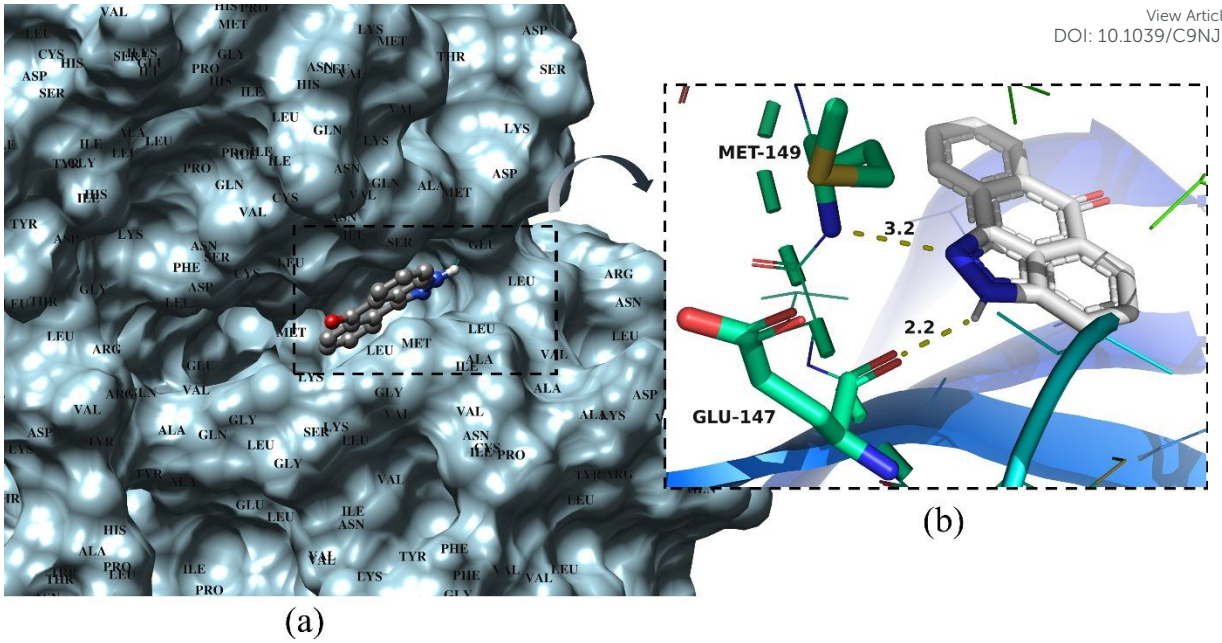

Figure 8 Mitogen-activated protein kinase 10 (JNK3) protein crystallized with dihydroanthrapyrazole (ATRP), one of its inhibitors (a). Binding model of ATRP into JNK3 obtained from our docking model (b). The RMSD between our ATRP calculated model and the crystallized compound is 1.063 Å, indicating a suitable theoretical method.

c-Jun N-terminal kinase (JNK) is a subfamily of mitogen-activated protein kinase (MAPK) with three differently spliced genes, namely, JNK1 (MAPK8), JNK2 (MAPK9), and JNK3 (MAPK10). Some diseases, such as cancer, inflammation, and neurodegenerative diseases, show over activation of JNK. JNK1 and JNK2 are expressed in various tissues, while JNK3 is restricted to testes, heart and brain. Expression of JNK3 is largely restricted to the brain as a tumor suppressor, and most of brain tumor presents loss of expression of the *jnk3* gene[2,50,51]. Considering this, the JKN3 protein was chosen as potential target for compounds **I-VIII**. Indeed, as will be shown in the experimental tests, this protein has straight relationship with one cell line tested.

Docking studies started with the active site ligand-based selection, which is a box with dimensions 14.5 Å x 20.5 Å x 18.1 Å centered at 20.29 Å x, 28.40 Å y and 20.57Å z. This model was validated by docking ATRP into this active site, which resulted in a RMSD = 1.063. In our model (and in the Scapin's work[49]), ATRP was found to inhibit JNK3 by interacting with both Glu147 (2.2 Å) and Met149 (3.2 Å) residues with binding affinity (BA) -9.1 kcal/mol. Figure 9 shows the structures of compounds **I-IX** docked into this same active site of JNK3, while their bindings modes are presented in Figure 9 and Table 3 presents the estimated BA, number of interactions (N_{HB}) and protein residues involved.

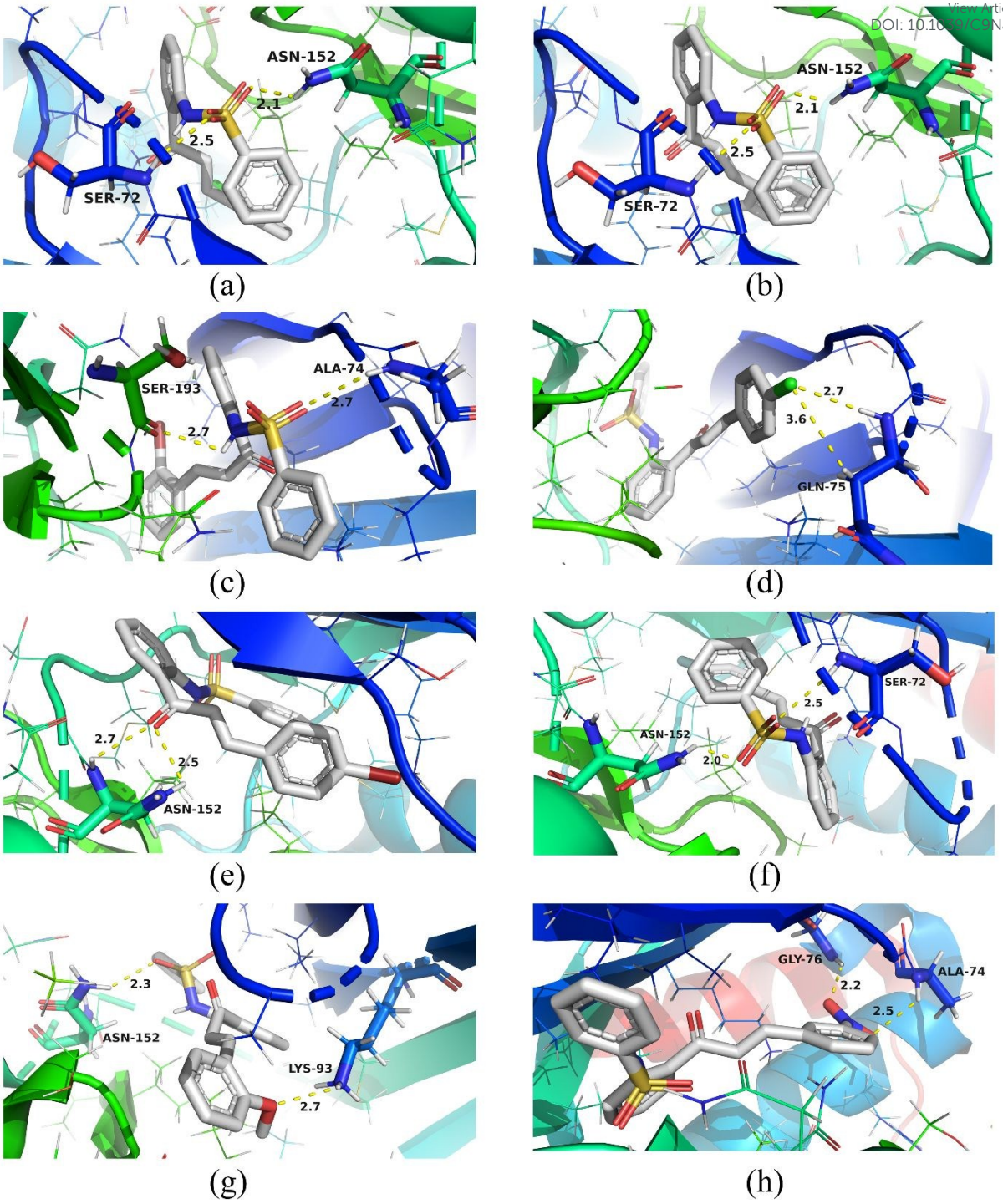

Figure 9 Binding modes of compounds **I** (a), **II** (b), **III** (c), **IV** (d), **V** (e), **VI** (f), **VII** (g) and **VIII** (h) into the active site of JNK3. For each item are shown the molecular poses, intermolecular interactions, residues and distances (in Å).

Table 5 Details on energy, quantity and residues of the binding modes of compounds **I-VIII** and ATRP, the standard inhibitor, into JNK3

Compound	Estimated BA	N_{HB}	Residues
I	-9.1 Kcal.mol^{-1}	2	Serine (SER) and Asparagine (ASN)
II	-9.5 Kcal.mol^{-1}	2	Serine (SER) and Asparagine (ASN)

View Article Online
DOI: 10.1039/C9NJ05612B

III	-9.6 Kcal.mol^{-1}	2	Serine (SER) and Alanine (ASN)
IV	-10.0 Kcal.mol^{-1}	2	Glutamine (GLN)
V	-8.8 Kcal.mol^{-1}	2	Asparagine (ASN)
VI	-9.8 Kcal.mol^{-1}	2	Serine (SER) and Asparagine (ASN)
VII	-9.2 Kcal.mol^{-1}	1	Asparagine (ASN) and Lysine (LYS)
VIII	-9.3 Kcal.mol^{-1}	2	Glycine (GLY) and Alanine (ALA)
ATRP	-9.1 Kcal.mol^{-1}	2	Glutamic acid (GLU) and Methionine (MET)

JNK3 is known to be inhibited through intermolecular interactions involving both GLU-147 and MET-149 residues. Although the most recent JNK3 inhibitors are from diarylimidazole family, ATP analogues and ATRP[49], some 3-substituted indoli-2-one[52], aminopyrazole[53] and trisubstituted thiophene derivatives[54] have been also studied for this purpose. Hereby, we present some sulfonamid -chalcones hybrids which could inhibit JNK3 via alternative residues, as seen in Figure 9. Both compounds **I** and **II** (Figures 9a and 9b) have similar binding modes, which involve two H Bonds (HB) between their sulfonyl group and SER-72 and ASN-152 with distances 2.1 Å and 2.5 Å, respectively. Because of differences on their poses, their BA are slightly different, both having similar or better values than ATRP. Interacting with SER-193 and ALA-74 through H_{AMINO} and $Os_{ULFONYL}$ with distances 2.7 Å, compound **III** was found to have better BA to JNK3 than ATPR (Figure 9c). Unlike **I-III**, the binding mode of **IV** is ruled by interactions between GLN-75 and the chlorine atom (2.7 Å and 3.6 Å; Figure 9d). With better BA to JNK3 (-10.0 Kcal.mol^{-1}) than ATRP and compounds **I-III** and **V-VIII**, we suggest that this halogen in the *para*-position plays key role on its biological potential. For **V**, it was observed one bifurcated interaction with JNK3 in which $O_{CARBONYL}$ acts as acceptor for ASN-152 hydrogens (2.5 and 2.7 Å, BA = -8.8 Kcal.mol^{-1}; Figure 9e). Besides also interacting with ASN-152, the sulfonyl group from compound **VI** stablishes one H bonding with SER-72 (2.0 Å and 2.5 Å, providing a BA = -8.8 Kcal.mol^{-1}; Figure 9f). Finally, compounds **VII** and **VIII** have different binding modes, both involving the substituent of the chalcone backbone: **VII** is accommodated into JNK3 active site through interactions involving $O_{SULFONYL}$···ASN-152 (2.3 Å) and $O_{ETHOXYL}$ ···LYS-93 (2.7 Å) (Figure 9g), while the nitro group of **VIII** interacts with GLY-76 (2.2 Å) and ALA-74 (2.5 Å) (Figure 9h). Both compounds **VII** and **VIII** showed better BA to JNK3 than ATRP, with values -9.2 Kcal.mol^{-1} and -9.2 Kcal.mol^{-1}, respectively.

Some studies demonstrate that activation of oncogenes such as Ras, c-fos, Met and Bcr-Abl may be JNK dependent, contributing to cellular transformation that supports cancer development. Whereas, JNK inhibitors are strong candidates for anticancer agent. Some JNK

inhibitors were approved and have been used to treat cancer, and others are in different phases of clinical study[2,50,51]. These compounds seem to affect the proliferation, adhesion and migration of some tumor cell lines, inducing cell cycle arrest and apoptosis, as well as, making these cells more sensitive to treatment with other chemotherapies[55–58]. In additions to cancer, some inhibitors are also used in inflammation[59] and as antiviral agent[60].

Warmka and collabolators[61]described the inhibitory effect of a chalcone analog on cell viability and NF-kB, with activation of caspases, and activation of extracellular signal regulated kinase 1/2 (ERK1/2) and c-Jun N-terminal kinase (JNK) in A549 lung cancer cells. When associated with a pharmacological inhibitor of ERK1/2 or JNK, these cells were more sensitive to chalcone-induced cytotoxicity without affecting NF-κB or caspase activity. Other studies showed that sulfonamides and their derivatives can activate or inhibit JNK pathway. The activation of this pathway can led to the induction of apoptosis of colorectal cancer cells[62,63], while the inhibition prevents neuronal cell death induced by growth factor and serum deprivation[64] . No studies have shown the effect of sulfonamide chalcones on the JNK pathway. Studies on the action of chalcones and sulfonamides on this pathway are still controversial. Thus, further investigation is required.

4. Theoretical Calculations

Theoretical calculations were performed in order to study the influence of different media on compounds **I-VIII**. Figure 10 shows overlays between the molecular conformations of **I-VIII** in the solid state (SS), aqueous-simulated medium (AS) and docking results (DS), adopting the aromatic ring A as fixed group. AS conformations (black) of all compounds were found to be relatively similar to SS conformations, with main discrepancy observed for benzenesulfonyl rings. In contrast, compounds **I**, **II**, **III**, **V**, **VI** and **VIII** adopt totally different conformation in SS and DS. These differences motivated us to calculate the energy of each conformation, energy gap between SS/AS (ΔE1) and energy gap between SS/DS (Table 3). For all compounds, the energy was found to increase following the sequence AS > DS > SS. Considering the energy to convert the SS conformation into that observed for DS, (ΔE2), compound **V** demands more energy (-7.620×10^2 kJ/mol) while the smallest energy was observed for compound **VI** (-6.961×10^2 kJ/mol).

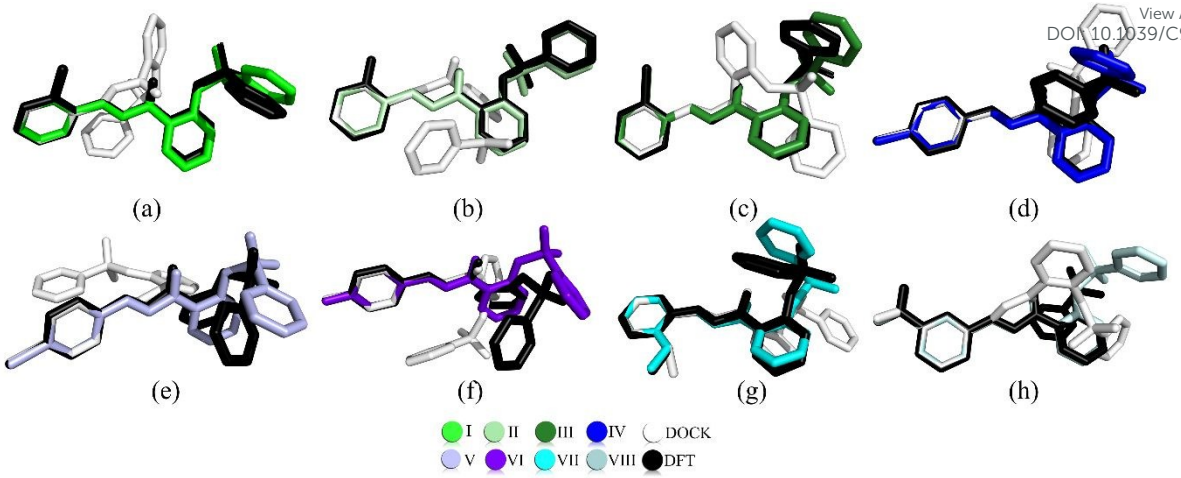

Figure 10 Overlay between the molecular conformations of **I** (a), **II** (b), **III** (c), **IV** (d), **V** (e), **VI** (f), **VII** (g) and **VIII** (h) in their solid state (SS), aqueous-simulated medium (black) and docking simulation (white). The aromatic ring A was kept fixed.

Table 6 Energy of each conformation in solid state (SS), aqueous-simulated medium (AS), docking results (DS), gap between SS/AS (ΔE1) and gap between SS/DS (ΔE2).

	Energy (kJ/mol)				
	SS (x10^6)	**AS (x10^6)**	**DS (x10^6)**	**ΔE1 (x10^3)**	**ΔE2 (x10^2)**
I	-5.127	-5.129	-5.127	-2.280	-7.024
II	-4.178	-4.181	-4.179	-2.313	-7.410
III	-10.692	-10.699	-10.693	-2.172	-7.282
IV	-5.126	-5.129	-5.127	-2.376	-7.330
V	-10.693	-10.698	-10.694	-2.335	-7.620
VI	-4.178	-4.181	-4.179	-2.346	-6.961
VII	-4.218	-4.221	-4.219	-2.426	-7.510
VIII	-4.455	-4.458	-4.456	-2.442	-7.209

5. Conclusion

After experimentally tested, our compounds were found to be cytotoxic against tumor cell lines SF-295 and PC-3, which motivated us to investigate the possible structural bases for this action. Topological analysis for our compounds was carried out through Hirshfeld analysis to identify intermolecular interactions sites, important also for protein-ligand analysis. Then, it was performed a structure-based pharmacophoric screening, which indicated that all sulfonamide chalcones are potential mitogen-activated protein kinase 10 (JNK3) inhibitors. Molecular docking simulations were used to investigate the binding model of our compounds, and they were found to interact with JNK3 with same or better binding

affinity than ATRP, one small molecule cocristallized with JNK3. Our findings allow further studies to confirm the mechanism involved in the antitumor effect of sulfonamide chalcones in order to develop new anti-cancer molecules. In addition, this work opens perspectives to evaluate the effect of sulfonamide chalcones against other diseases which the JNK pathway is also involved, such as inflammation and neurodegeneration.

6. Acknowledgements

The authors thank to Coordenação de Aperfeiçoamento de Pessoal de Nível Superior (CAPES) and Conselho Nacional de Desenvolvimento Científico e Tecnológico (CNPq) for the financial support. Research developed with support of the High Performance Computing Center at the Universidade Estadual de Goiás (UEG).

7. References

(1) Baudino, T. Targeted Cancer Therapy: The Next Generation of Cancer Treatment. *Curr. Drug Discov. Technol.* **2015**, *12* (1), 3–20. https://doi.org/10.2174/1570163812666150602144310.

(2) Bubici, C.; Papa, S. JNK Signalling in Cancer: In Need of New, Smarter Therapeutic Targets. *Br. J. Pharmacol.* **2014**, *171* (1), 24–37. https://doi.org/10.1111/bph.12432.

(3) Siddiqui, M. A.; Reddy, P. A. Small Molecule JNK (c-Jun N-Terminal Kinase) Inhibitors. *J. Med. Chem.* **2010**, *53* (8), 3005–3012. https://doi.org/10.1021/jm9003279.

(4) MAGALHAES, L. G.; FERREIRA, L. L. G.; ANDRICOPULO, A. D. Recent Advances and Perspectives in Cancer Drug Design. *An. Acad. Bras. Cienc.* **2018**, *90*, 1233–1250. https://doi.org/10.1590/0001-3765201820170823.

(5) Byrne, R.; Schneider, G. In Silico Target Prediction for Small Molecules. *Methods Mol. Biol.* **2019**, *1888*, 273–309. https://doi.org/10.1007/978-1-4939-8891-4_16.

(6) Manvara, P.; Kapadiyab, K.; Kavadiab, K.; Munshib, K.; Khuntb, R. Screening of Some Novel Cyanopyridine CHEMISTRY & BIOLOGY INTERFACE. *Chem. Biol. INTERFACE* **2015**, *5* (5), 324–332.

(7) Olivella, M. S.; Zarelli, V. E. P.; Pappano, N. B.; Debattista, N. B. A COMPARATIVE STUDY OF BACTERIOSTATIC ACTIVITY OF SYNTHETIC HYDROXYLATED FLAVONOIDS. *Brazilian J. Microbiol.* **2001**, 229–232.

(8) Damazio, R. G.; Zanatta, A. P.; Cazarolli, L. H.; Mascarello, A.; Chiaradia, L. D.; Nunes, R. J.; Yunes, R. A.; Silva, F. R. M. B. Nitrochalcones: Potential in Vivo Insulin Secretagogues. *Biochimie* **2009**, *91* (11–12), 1493–1498. https://doi.org/10.1016/j.biochi.2009.09.002.

(9) Wang, J.; Wang, S.; Song, D.; Zhao, D.; Sha, Y.; Jiang, Y.; Jing, Y.; Cheng, M. Chalcone

Derivatives Inhibit Glutathione S-Transferase P1-1 Activity: Insights into the Interaction Mode of ??, ??-Unsaturated Carbonyl Compounds. *Chem. Biol. Drug Des.* **2009**, *73* (5), 511–514. https://doi.org/10.1111/j.1747-0285.2009.00807.x.

(10) Solomon, V. R.; Lee, H. Anti-Breast Cancer Activity of Heteroaryl Chalcone Derivatives. *Biomed. Pharmacother.* **2012**, *66* (3), 213–220. https://doi.org/10.1016/j.biopha.2011.11.013.

(11) Marković, V.; Debeljak, N.; Stanojković, T.; Kolundžija, B.; Sladić, D.; Vujčić, M.; Janović, B.; Tanić, N.; Perović, M.; Tešić, V.; et al. Anthraquinone-Chalcone Hybrids: Synthesis, Preliminary Antiproliferative Evaluation and DNA-Interaction Studies. *Eur. J. Med. Chem.* **2015**, *89*, 401–410. https://doi.org/10.1016/j.ejmech.2014.10.055.

(12) Nowakowska, Z. A Review of Anti-Infective and Anti-Inflammatory Chalcones. *Eur. J. Med. Chem.* **2007**, *42* (2), 125–137. https://doi.org/10.1016/j.ejmech.2006.09.019.

(13) Nowakowska, Z.; Kedzia, B.; Schroeder, G. Synthesis , Physicochemical Properties and Antimicrobial Evaluation of New (E) -Chalcones. *Eur. J. Med. Chem. 43* **2008**, *43*, 707–713. https://doi.org/10.1016/j.ejmech.2007.05.006.

(14) Coa, J. C.; García, E.; Carda, M.; Agut, R.; Vélez, I. D.; Muñoz, J. A.; Yepes, L. M.; Robledo, S. M.; Cardona, W. I. Synthesis, Leishmanicidal, Trypanocidal and Cytotoxic Activities of Quinoline-Chalcone and Quinoline-Chromone Hybrids. *Med. Chem. Res.* **2017**, *26* (7), 1405–1414. https://doi.org/10.1007/s00044-017-1846-5.

(15) Monserrat, J. P.; Al-Safi, R. I.; Tiwari, K. N.; Quentin, L.; Chabot, G. G.; Vessires, A.; Jaouen, G.; Neamati, N.; Hillard, E. A. Ferrocenyl Chalcone Difluoridoborates Inhibit HIV-1 Integrase and Display Low Activity towards Cancer and Endothelial Cells. *Bioorganic Med. Chem. Lett.* **2011**, *21* (20), 6195–6197. https://doi.org/10.1016/j.bmcl.2011.07.078.

(16) Silva, C. R. e; Borges, F. F. V.; Bernardes, A.; Perez, C. N.; Silva, D. de M. e; Chen-Chen, L. Genotoxic, Cytotoxic, Antigenotoxic, and Anticytotoxic Effects of Sulfonamide Chalcone Using the Ames Test and the Mouse Bone Marrow Micronucleus Test. *PLoS One* **2015**, *10* (9), e0137063. https://doi.org/10.1371/journal.pone.0137063.

(17) Bahekar, S. P.; Hande, S. V.; Agrawal, N. R.; Chandak, H. S.; Bhoj, P. S.; Goswami, K.; Reddy, M. V. R. Sulfonamide Chalcones: Synthesis and in Vitro Exploration for Therapeutic Potential against Brugia Malayi. *Eur. J. Med. Chem.* **2016**, *124*, 262–269. https://doi.org/10.1016/j.ejmech.2016.08.042.

(18) Domínguez, J. N.; León, C.; Rodrigues, J.; Gamboa, N.; Domínguez, D. Synthesis and Antimalarial Activity of Sulfonamide Chalcone Derivatives. *Farm.* **2005**, *60*, 307–311. https://doi.org/10.1016/j.farmac.2005.01.005.

(19) Noreljaleel, A. E. M.; Wilhelm, A.; Bonnet, S. L.; van der Westhuizen, J. H. Synthesis and Bioactivity of Reduced Chalcones Containing Sulfonamide Side Chains. *J. Nat. Prod.* **2018**, *81* (1), 41–48. https://doi.org/10.1021/acs.jnatprod.7b00570.

(20) Bonakdar, A. P. S.; Vafaei, F.; Farokhpour, M.; Esfahani, M. H. N.; Massah, A. R. Synthesis

and Anticancer Activity Assay of Novel Chalcone-Sulfonamide Derivatives. *Iran J Pharm Res.* **2017**, *16* (2), 565–568.

(21) Seo, W. D.; Kim, J. H.; Kang, J. E.; Ryu, H. W.; Curtis-Long, M. J.; Lee, H. S.; Yang, M. S.; Park, K. H. Sulfonamide Chalcone as a New Class of α-Glucosidase Inhibitors. *Bioorg. Med. Chem. Lett.* **2005**, *15* (24), 5514–5516. https://doi.org/10.1016/j.bmcl.2005.08.087.

(22) Kang, J.; Cho, J.; Curtis-Long, M.; Ryu, H.; Kim, J.; Kim, H.; Yuk, H.; Kim, D.; Park, K. Inhibitory Evaluation of Sulfonamide Chalcones on β-Secretase and Acylcholinesterase. *Molecules* **2012**, *18* (1), 140–153. https://doi.org/10.3390/molecules18010140.

(23) Arslan, T.; Türkoğlu, E. A.; Şentürk, M.; Supuran, C. T. Synthesis and Carbonic Anhydrase Inhibitory Properties of Novel Chalcone Substituted Benzenesulfonamides. *Bioorg. Med. Chem. Lett.* **2016**, *26* (24), 5867–5870. https://doi.org/10.1016/j.bmcl.2016.11.017.

(24) Peerzada, M. N.; Khan, P.; Ahmad, K.; Hassan, M. I.; Azam, A. Synthesis, Characterization and Biological Evaluation of Tertiary Sulfonamide Derivatives of Pyridyl-Indole Based Heteroaryl Chalcone as Potential Carbonic Anhydrase IX Inhibitors and Anticancer Agents. *Eur. J. Med. Chem.* **2018**, *155*, 13–23. https://doi.org/10.1016/j.ejmech.2018.05.034.

(25) Ejaz, S. A.; Saeed, A.; Siddique, M. N.; Nisa, Z. un; Khan, S.; Lecka, J.; Sévigny, J.; Iqbal, J. Synthesis, Characterization and Biological Evaluation of Novel Chalcone Sulfonamide Hybrids as Potent Intestinal Alkaline Phosphatase Inhibitors. *Bioorg. Chem.* **2017**, *70*, 229–236. https://doi.org/10.1016/j.bioorg.2017.01.003.

(26) McKinnon, J. J.; Turner, M. J.; Jayatilaka, D.; Spackman, M. A.; Grimwood, D. J.; Wolff, S. K. Crystal Explorer (Version 3.1). University of Western Australia 2012.

(27) McKinnon, J. J.; Spackman, M. a.; Mitchell, A. S. *Novel Tools for Visualizing and Exploring Intermolecular Interactions in Molecular Crystals*; 2004; Vol. 60. https://doi.org/10.1107/S0108768104020300.

(28) Custodio, J. M. F.; Faria, E. C. M.; Sallum, L. O.; Duarte, V. S.; Vaz, W. F.; De Aquino, G. L. B.; Carvalho, P. S.; Napolitano, H. B. The Influence of Methoxy and Ethoxy Groups on Supramolecular Arrangement of Two Methoxy-Chalcones. *Artic. J. Braz. Chem. Soc* **2017**, *00* (00), 1–12. https://doi.org/10.21577/0103-5053.20170067.

(29) Custodio, J. M. F.; Ternavisk, R. R.; Ferreira, C. J. S.; Figueredo, A. S.; Aquino, G. L. B.; Napolitano, H. B.; Valverde, C.; Baseia, B. Using the Supermolecule Approach To Predict the Nonlinear Optics Potential of a Novel Asymmetric Azine. *J. Phys. Chem. A* **2019**, *123* (1), 153–162. https://doi.org/10.1021/acs.jpca.8b07872.

(30) Custodio, J. M. F.; Moreira, C. A.; Valverde, C.; De Aquino, G. L. B.; Baseiaa, B.; Napolitano, H. B. Hirshfeld Surfaces and Nonlinear Optics on Two Conformers of a Heterocyclic Chalcone. *J. Braz. Chem. Soc.* **2018**, *29* (2). https://doi.org/10.21577/0103-5053.20170136.

(31) Spackman, M. A.; McKinnon, J. J. Fingerprinting Intermolecular Interactions in Molecular

Crystals. *CrystEngComm* **2002**, *4* (66), 378–392. https://doi.org/10.1039/B203191B.

(32) Wang, X.; Shen, Y.; Wang, S.; Li, S.; Zhang, W.; Liu, X.; Lai, L.; Pei, J.; Li, H. PharmMapper 2017 Update: A Web Server for Potential Drug Target Identification with a Comprehensive Target Pharmacophore Database. *Nucleic Acids Res.* **2017**, *45* (W1), W356–W360. https://doi.org/10.1093/nar/gkx374.

(33) Hawkins, P. C. D.; Skillman, A. G.; Warren, G. L.; Ellingson, B. A.; Stahl, M. T. Conformer Generation with OMEGA: Algorithm and Validation Using High Quality Structures from the Protein Databank and Cambridge Structural Database. *J. Chem. Inf. Model.* **2010**, *50* (4), 572–584. https://doi.org/10.1021/ci100031x.

(34) OMEGA v.2.5.1: OpenEye Scientific Software, Santa Fe, NM. Http://Www.Eyesopen.Com.

(35) Jakalian, A.; Jack, D. B.; Bayly, C. I. Fast, Efficient Generation of High-Quality Atomic Charges. AM1-BCC Model: II. Parameterization and Validation. *J. Comput. Chem.* **2002**, *23* (16), 1623–1641. https://doi.org/10.1002/jcc.10128.

(36) QUACPAC v.1.6.3: OpenEye Scientific Software, Santa Fe, NM. Http://Www.Eyesopen.Com.

(37) Anandakrishnan, R.; Aguilar, B.; Onufriev, A. V. H++ 3.0: Automating PK Prediction and the Preparation of Biomolecular Structures for Atomistic Molecular Modeling and Simulations. *Nucleic Acids Res.* **2012**, *40* (W1), W537–W541. https://doi.org/10.1093/nar/gks375.

(38) Gordon, J. C.; Myers, J. B.; Folta, T.; Shoja, V.; Heath, L. S.; Onufriev, A. H++: A Server for Estimating PKas and Adding Missing Hydrogens to Macromolecules. *Nucleic Acids Res.* **2005**, *33* (Web Server), W368–W371. https://doi.org/10.1093/nar/gki464.

(39) Trott, O.; Olson, A. J. AutoDock Vina: Improving the Speed and Accuracy of Docking with a New Scoring Function, Efficient Optimization, and Multithreading. *J. Comput. Chem.* **2010**, *31* (2), 455–461. https://doi.org/10.1002/jcc.21334.

(40) Hunter, C. A.; Sanders, J. K. M. The Nature of .Pi.-.Pi. Interactions. *J. Am. Chem. Soc.* **1990**, *112* (14), 5525–5534. https://doi.org/10.1021/ja00170a016.

(41) de Castro, M. R. C.; Naves, R. F.; Bernardes, A.; da Silva, C. C.; Perez, C. N.; Moura, A. F.; de Moraes, M. O.; Martins, F. T. Tandem Chalcone-Sulfonamide Hybridization, Cyclization and Further Claisen–Schmidt Condensation: Tuning Molecular Diversity through Reaction Time and Order and Catalyst. *Arab. J. Chem.* **2017**. https://doi.org/10.1016/j.arabjc.2017.11.005.

(42) Custodio, J. M. F.; Vaz, W. F.; de Castro, M. R. C.; Bernardes, A.; Naves, R. F.; Moura, A. F.; de Moraes, M. O.; da Silva, C. C.; Martins, F. T.; Perez, C. N.; et al. Solvent-Driven Structural Adaptation in a Novel Anticancer Sulfonamide Chalcone. *J. Mol. Struct.* **2019**, *1175*, 389–397. https://doi.org/10.1016/j.molstruc.2018.07.059.

(43) Custodio, J.; Michelini, L.; Castro, M.; Fonseca Vaz, W.; Neves, B. J.; Cravo, P.; Barreto, F.; de Moraes, M. O.; Perez, C.; Napolitano, H. Structural Insights on a Novel Anticancer

Sulfonamide Chalcone. *New J. Chem.* **2018**, 1–9. https://doi.org/10.1039/C7NJ03523C.

(44) d'Oliveira, G.; Moura, A.; de Moraes, M.; Perez, C.; Lião, L. Synthesis, Characterization and Evaluation of in Vitro Antitumor Activities of Novel Chalcone-Quinolinone Hybrid Compounds. *J. Braz. Chem. Soc.* **2018**, *29* (11), 2308–2325. https://doi.org/10.21577/0103-5053.20180108.

(45) Ghorab, M. M.; Ragab, F. A.; Heiba, H. I.; El-Gazzar, M. G.; Zahran, S. S. Synthesis, Anticancer and Radiosensitizing Evaluation of Some Novel Sulfonamide Derivatives. *Eur. J. Med. Chem.* **2015**, *92*, 682–692. https://doi.org/10.1016/j.ejmech.2015.01.036.

(46) Custodio, J. M. F.; Michelini, L. J.; De Castro, M. R. C.; Vaz, W. F.; Neves, B. J.; Cravo, P. V. L.; Barreto, F. S.; Filho, M. O. M.; Perez, C. N.; Napolitano, H. B. Structural Insights into a Novel Anticancer Sulfonamide Chalcone. *New J. Chem.* **2018**, *42* (5). https://doi.org/10.1039/c7nj03523c.

(47) Wang, X.; Pan, C.; Gong, J.; Liu, X.; Li, H. Enhancing the Enrichment of Pharmacophore-Based Target Prediction for the Polypharmacological Profiles of Drugs. *J. Chem. Inf. Model.* **2016**, *56* (6), 1175–1183. https://doi.org/10.1021/acs.jcim.5b00690.

(48) Liu, X.; Ouyang, S.; Yu, B.; Liu, Y.; Huang, K.; Gong, J.; Zheng, S.; Li, Z.; Li, H.; Jiang, H. PharmMapper Server: A Web Server for Potential Drug Target Identification Using Pharmacophore Mapping Approach. *Nucleic Acids Res.* **2010**, *38* (suppl_2), W609–W614. https://doi.org/10.1093/nar/gkq300.

(49) Scapin, G.; Patel, S. B.; Lisnock, J.; Becker, J. W.; LoGrasso, P. V. The Structure of JNK3 in Complex with Small Molecule Inhibitors. *Chem. Biol.* **2003**, *10* (8), 705–712. https://doi.org/10.1016/S1074-5521(03)00159-5.

(50) Cicenas, J.; Zalyte, E.; Rimkus, A.; Dapkus, D.; Noreika, R.; Urbonavicius, S. JNK, P38, ERK, and SGK1 Inhibitors in Cancer. *Cancers (Basel).* **2017**, *10* (1), 1. https://doi.org/10.3390/cancers10010001.

(51) Yang, D. D.; Kuan, C.-Y.; Whitmarsh, A. J.; Rinócn, M.; Zheng, T. S.; Davis, R. J.; Rakic, P.; Flavell, R. A. Absence of Excitotoxicity-Induced Apoptosis in the Hippocampus of Mice Lacking the Jnk3 Gene. *Nature* **1997**, *389* (6653), 865–870. https://doi.org/10.1038/39899.

(52) Dou, X.; Huang, H.; Li, Y.; Jiang, L.; Wang, Y.; Jin, H.; Jiao, N.; Zhang, L.; Zhang, L.; Liu, Z. Multistage Screening Reveals 3-Substituted Indolin-2-One Derivatives as Novel and Isoform-Selective c-Jun N-Terminal Kinase 3 (JNK3) Inhibitors: Implications to Drug Discovery for Potential Treatment of Neurodegenerative Diseases. *J. Med. Chem.* **2019**, *62* (14), 6645–6664. https://doi.org/10.1021/acs.jmedchem.9b00537.

(53) Zheng, K.; Iqbal, S.; Hernandez, P.; Park, H.; LoGrasso, P. V.; Feng, Y. Design and Synthesis of Highly Potent and Isoform Selective JNK3 Inhibitors: SAR Studies on Aminopyrazole Derivatives. *J. Med. Chem.* **2014**, *57* (23), 10013–10030. https://doi.org/10.1021/jm501256y.

(54) Wu, X.-X.; Dai, D.-S.; Zhu, X.; Li, X.-F.; Yuan, J.; Wu, X.-F.; Miao, M.-S.; Zeng, H.-H.;

Zhao, C.-L. Molecular Modeling Studies of JNK3 Inhibitors Using QSAR and Docking. *Med. Chem. Res.* **2014**, *23* (5), 2456–2475. https://doi.org/10.1007/s00044-013-0782-2.

(55) Cerbone, A.; Toaldo, C.; Minelli, R.; Ciamporcero, E.; Pizzimenti, S.; Pettazzoni, P.; Roma, G.; Dianzani, M. U.; Ullio, C.; Ferretti, C.; et al. Rosiglitazone and AS601245 Decrease Cell Adhesion and Migration through Modulation of Specific Gene Expression in Human Colon Cancer Cells. *PLoS One* **2012**, *7* (6), e40149. https://doi.org/10.1371/journal.pone.0040149.

(56) Cerbone, A.; Toaldo, C.; Pizzimenti, S.; Pettazzoni, P.; Dianzani, C.; Minelli, R.; Ciamporcero, E.; Roma, G.; Dianzani, M. U.; Canaparo, R.; et al. AS601245, an Anti-Inflammatory JNK Inhibitor, and Clofibrate Have a Synergistic Effect in Inducing Cell Responses and in Affecting the Gene Expression Profile in CaCo-2 Colon Cancer Cells. *PPAR Res.* **2012**, *1*, 1–16. https://doi.org/10.1155/2012/269751.

(57) Cui, J.; Wang, Q.; Wang, J.; Lv, M.; Zhu, N.; Li, Y.; Feng, J.; Shen, B.; Zhang, J. Basal C-Jun NH2-Terminal Protein Kinase Activity Is Essential for Survival and Proliferation of T-Cell Acute Lymphoblastic Leukemia Cells. *Mol. Cancer Ther.* **2009**, *8* (12), 3214–3222. https://doi.org/10.1158/1535-7163.MCT-09-0408.

(58) Ramos, A. M.; Fernandez, C.; Amrán, D.; Esteban, D.; de Blas, E.; Palacios, M. A.; Aller, P. Pharmacologic Inhibitors of Extracellular Signal-Regulated Kinase (ERKs) and c-Jun NH2-Terminal Kinase (JNK) Decrease Glutathione Content and Sensitize Human Promonocytic Leukemia Cells to Arsenic Trioxide-Induced Apoptosis. *J. Cell. Physiol.* **2006**, *209* (3), 1006–1015. https://doi.org/10.1002/jcp.20806.

(59) Gaillard, P.; Jeanclaude-Etter, I.; Ardissone, V.; Arkinstall, S.; Cambet, Y.; Camps, M.; Chabert, C.; Church, D.; Cirillo, R.; Gretener, D.; et al. Design and Synthesis of the First Generation of Novel Potent, Selective, and in Vivo Active (Benzothiazol-2-Yl)Acetonitrile Inhibitors of the c-Jun N-Terminal Kinase. *J. Med. Chem.* **2005**, *48* (14), 4596–4607. https://doi.org/10.1021/jm0310986.

(60) Wolschendorf, F.; Bosque, A.; Shishido, T.; Duverger, A.; Jones, J.; Planelles, V.; Kutsch, O. Kinase Control Prevents HIV-1 Reactivation in Spite of High Levels of Induced NF-KB Activity. *J. Virol.* **2012**, *86* (8), 4548–4558. https://doi.org/10.1128/JVI.06726-11.

(61) Warmka, J. K.; Solberg, E. L.; Zeliadt, N. A.; Srinivasan, B.; Charlson, A. T.; Xing, C.; Wattenberg, E. V. Inhibition of Mitogen Activated Protein Kinases Increases the Sensitivity of A549 Lung Cancer Cells to the Cytotoxicity Induced by a Kava Chalcone Analog. *Biochem. Biophys. Res. Commun.* **2012**, *424* (3), 488–492. https://doi.org/10.1016/j.bbrc.2012.06.140.

(62) Ahmad, M. Evaluation of Neuro-Pharmacological Activities in Six Homeopathic Drugs. **2015**, *9* (11), 367–374. https://doi.org/10.5897/AJPP2015.

(63) Ahmad, R.; Vaali-Mohammed, M.; Elwatidy, M.; Al-Obeed, O.; Al-Khayal, K.; Eldehna, W.; Abdel-Aziz, H.; Alafeefy, A.; Abdulla, M. Induction of ROS-mediated Cell Death and Activation of the JNK Pathway by a Sulfonamide Derivative. *Int. J. Mol. Med.* **2019**, *44* (4),

1552–1562. https://doi.org/10.3892/ijmm.2019.4284.

View Article Online
DOI: 10.1039/C9NJ05612B

(64) Rückle, T.; Biamonte, M.; Grippi-Vallotton, T.; Arkinstall, S.; Cambet, Y.; Camps, M.; Chabert, C.; Church, D. J.; Halazy, S.; Jiang, X.; et al. Design, Synthesis, and Biological Activity of Novel, Potent, and Selective (Benzoylaminomethyl)Thiophene Sulfonamide Inhibitors of c-Jun-N-Terminal Kinase. *J. Med. Chem.* **2004**, *47* (27), 6921–6934. https://doi.org/10.1021/jm031112e.